Journal of Korean Institute of surface Engineering
Vol. 29, No. 6, Dec., 1996

OBSERVATION OF MICRO-STRUCTURE AND OPTICAL PROPERTISE OF TITANIUM DIOXIDE THIN FILMS USING OPTICAL MMEHODS

S.Y. Kim and H.J. Kim

Department of Physics, Ajou University, Suwon, Korea 442-749

ABSTRACT

TiO_2 films prepared by RF magnetron sputtering, electron beam evaporation, ion assisted deposition (IAD) and sol-gel method are prepared on c-Si substrate and vitreous silica substrate respectively. From the transmission spectra of TiO_2 films on vitreous silica substrate in the spectral region from 190 nm to 900 nm, $k(\lambda)$ of TiO_2 is obtained. Using $k(\lambda)$ in the interband transition region the coefficients of the quantum mechanical dispersion relation of an amorphous TiO_2 and hence $n(\lambda)$ including the optically opaque region of above fundamental transition energy are obtained. The spectroscopic ellipsometry spectra of TiO_2 films in the spectral region of 1.5-5.0eV are model analyzed to get the film packing density variation versus i) substrate material, ii) film thickness and iii) film growth technique. The complex refractive index change of these TiO_2 films versus water condensation is also studied. Film micro-structures by SE modelling results are compared with those by atomic force microscopy images and X-ray diffraction data.

INTRODUCTION

Although its intensive use as the high refractive index optical coating material,[1] titanium dioxide is still under investigation even about its very fundamental optical properties like refractive index and extinction coefficient.[2] Futhermore optical properties of TiO_2 in film phase is not clearly answered, partly because they strongly depend on film growth technique and film growing environment. Most TiO_2 films grown in room temperature show amorphous phase and they are hardly free from inhomogeneity, scattering, and surface micro-roughness.[2] Moreover, above the fundamental transition energy, it strongly absorbs light and hence at photon energy region above 3.5eV, the refractive index shows an anomalous dispersion. The extinction coefficient increases rapidly starting about 3.3eV and then shows a broad plateu like feature with a broad double peaks above 4.2eV.[3,4] Since TiO_2 film strongly absorbes light above band gap, the optical characterization of TiO_2 film above band gap region is quite similar to the determination of n and k of metal films or semiconductor films. Quite recently, the authors reported a method to characterize TiO_2 film using optical methods,[4] where the complex refractive index dispersion $n(\lambda)$ and $k(\lambda)$ of void-free TiO_2 in film phase has been presented.[5]

In the present work, this method is briefly reviewed where a double oscillator is introduced so that an accurate complex refractive index dispersion of TiO_2 film can be manipulated. Modelling SE data enabled to find the void distribution and the film thickness. The film microstructure in terms of packing density and surface microroughness are also addressed. The variation of the film packing density versus i) substrate material, ii) film thickness and iii) film growth technique are addressed. The effect of water condensation on the film index change together with film micro-structures by SE modelling and by atomic force microscopy are studied. The in-situ ellipsometric observation of the water desorption from the micro-void of TiO_2 film at the elevated temperature is also made.

EXPERIMENTAL

TiO_2 films are grown by a conventional electron beam evaporation, IAD, and RF sputtering, and sol-gel method respectively. The film thickness ranged from 500 Å to 3200 Å. The vitreous silica (ESCO Q610188) and c-Si wafer are used as substrate. The films on c-Si sustrate are for the SE analysis and the other films on vitreous silica substrate are for the transmission experiment and spectroellipsometric analysis. The spectral range of the spectroscopic ellipsometer (Jobin Yvon, UVISEL) is 1.5−5.5 eV. That of the spectrophotometer (JASCO V550) is 190-900 nm. The electron beam deposition is made by using a commercial type vacuum coater (Leybold A700Q), which is equipped with a closed cycle Freon refrigerator and a substrate heater. During the electron beam deposition substrate temperature is maintained at about 350 ℃. Argon ions from the Kaufmann ion source are used for IAD. The kinetic energy of argon ion is 400eV and the ion beam current is 25 $\mu A/cm^2$ respectively. Ar pressure of the RF sputtering chamber (Leybold L560) is kept under 5×10^{-3} mbar. RF power is 300W. The substrate was not heated during sputtering. During the film growth, film thickness is monitored by an oscillating quartz microbalance. For a direct observation of the surface microroughness, AFM (PSI Autoprobe LS) images are collected. The X-ray diffraction data is also collected to verify the amorphous film.

RESULTS AND DISCUSSION

TiO_2 films are transparent in optical region below the fundamental transition energy. The transmittance of 1117−Å-thick TiO_2 film on vitreous silica substrate is copied into Fig.1. Above 350 nm, an oscillatory behavior due to the interference of light by TiO_2 film is observed. Below 350 nm the transmittance decreases quite fast until it approaches nearly zero around 290 nm, below which TiO_2 film strongly absorbs light. Meanwhile it is well established how to model determine the optical properties and the void distribution of an unknown transparent thin film by analyzing SE data.[6] TiO_2 films are transparent at wavelengths longer than 350 nm, and hence SE data below the fundamental transition energy are analyzed according to such a method. Even with this limited SE data below the fundamental transition energy, the void distribution could be model determined, but only

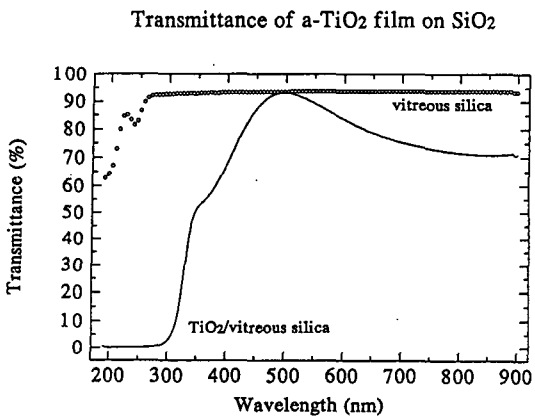

Fig. 1 The transmission spectrum of TiO_2 film on vitreous silica substrate. The oscillatory behavior above 350 nm is due to the interference of light by TiO_2 film. Below 350 nm the transmittance decreases quite fast until it approaches nearly zero around 290nm, below which TiO_2 film strongly absorbs light.

the film thickness is fetched for the reason which will be explained in a detail later. The optical model of TiO_2 film on a vitreous silica substrate for the determination of the film thickness is a three phase system consisted of air/film/substrate/air. With this film thickness, the extinction coefficient $k(\lambda)$ of the TiO_2 film of this three phase system is calculated by numerically inverting the transmittance according to the Eq.(1).[4]

$$k(\lambda)=-\frac{\lambda}{\pi d}\left[\ln(Tn_0)+\ln(1-|\gamma_2\gamma_3|^2)/(1-r_3^2)+\ln|(1+\gamma_1\gamma_2 e^{2i\delta})/t_1t_2|^2\right]$$

where T is the transmittance, n_0 is the substrate refractive index, $\delta=2\pi d(n+ik)/\lambda$, and d is the film thickness. t_1, t_2 are the Fresnel transmission coefficients at air/film and film/substrate interfaces respectively. γ_1, γ_2 are the Fresnel reflection coefficients at the same interfaces. γ_3 is the Fresnel reflection coefficient at substrate/air interface. The inverted equation in Eq.(1) is practically useful to get $k(\lambda)$ at interband transition region. Note that $k(\lambda)$ is implicitly included in the right hand side of Eq.(1) and hence it should be determined by iteration. For large $k(>\lambda/10d)$, the dominant contribution comes from the first term in the bracket, hence only a few iteration is enough to get the rapid convergence of $k(\lambda)$ in which the contribution from the other terms are properly accounted for. The calculated extinction coefficients of TiO_2 films above the fundamental transition energy rise from zero at 3.3 eV to 1.14~1.48 around 5.0eV and after that it decrease very slowly. The extinction coefficient spectra of films thinner than 1100Å, are shown in Fig. 2. The shape of $k(\lambda)$ spectrum is similar to each other except the height difference. The higher $k(\lambda)$ is attributed to the denser film. Denser films show higher extinction coefficients above band gap, which is quite similar

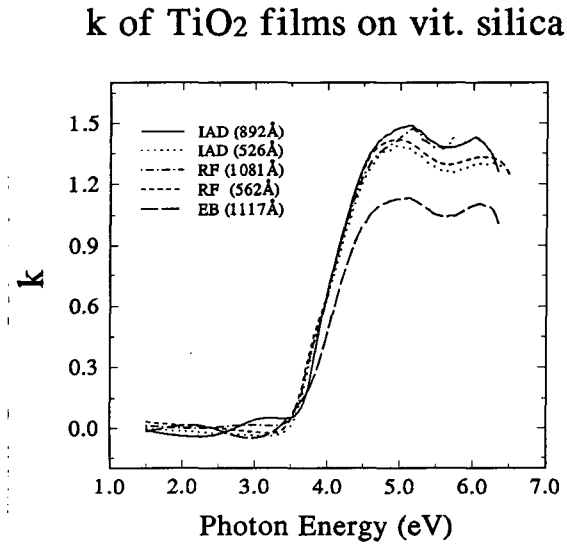

Fig. 2. The extinction coefficent of TiO_2 films on vitreous silica substrate, prepared by conventional electron beam evaporation IAD and RF sputtering. The extinction coefficient of TiO_2 films thicker than 1100 Å are not included for the reason explained in the text.

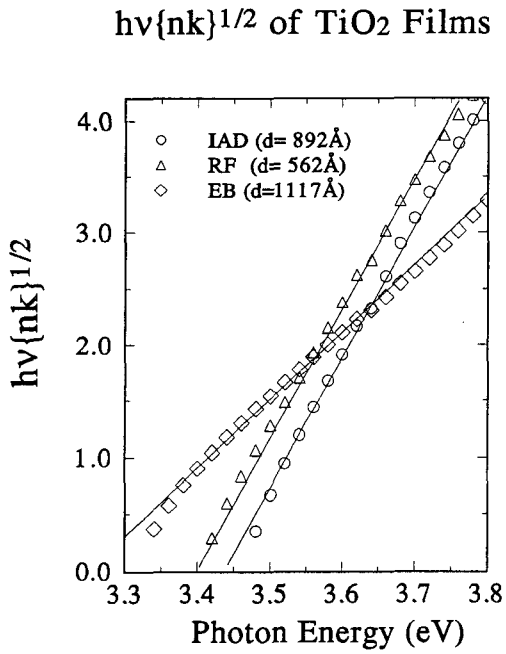

Fig. 3. The graph of $h\nu\sqrt{nk}$ vs $h\nu$ of TiO_2 films prepared by conventional electron beam deposition, IAD and RF sputtering near the fundamental transition energy. The x-intersection of the best fit line is identified as the band agp.

to the fact that below band gap, denser films have higher refractive index values. From the refractive index variation, film packing density variation can be derived. Rhis will be discussed later. Thick films absorbs light such that the transmitted light is too weak to be detected by the spectrophotometer. From the inverted $\boldsymbol{k}(\lambda)$ above the fundamental transition energy, plots of $h\nu\sqrt{nk}$ vs $h\nu$ are made (Fig.3) and the x-intersection of the best fit line to this plot are obtained. The band gap of TiO_2 film is identified as the x-intersection of the best fit lines of$h\nu\sqrt{nk}$ versus $h\nu$ above the fundamental transition energy. As shown in Fig. 4, they scatter around 3.35eV. Electron beam grown TiO_2 films (3.37 eV) show greater values than sputter grown ones (3.32 eV).

The TiO_2 films are amorphous, which are confirmed by the X-ray diffraction data. Fig. 5 shows a typical θ-2θ data, where no sign of crystallinity in the film can be found. The complex refractive index of an amorphous material can be expressed in terms of a quantum mechanical dispersion relation, hence the calculated $k(\lambda)$ is least square fitted to the

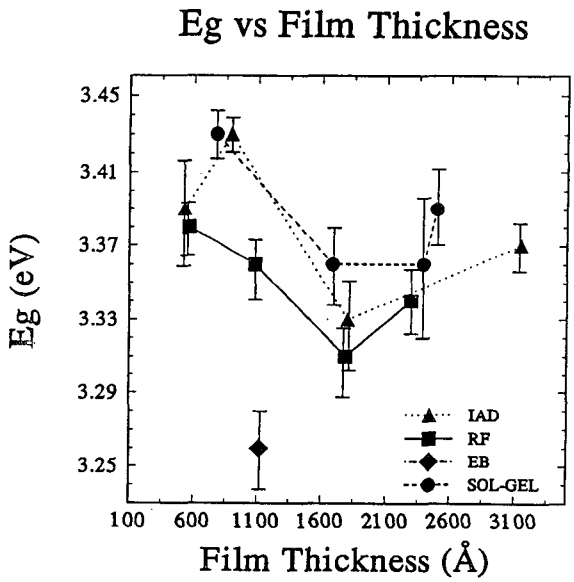

Fig. 4. The band gap of TiO_2 films prepared by RF, IAD, electron beam and sop-gel technique.

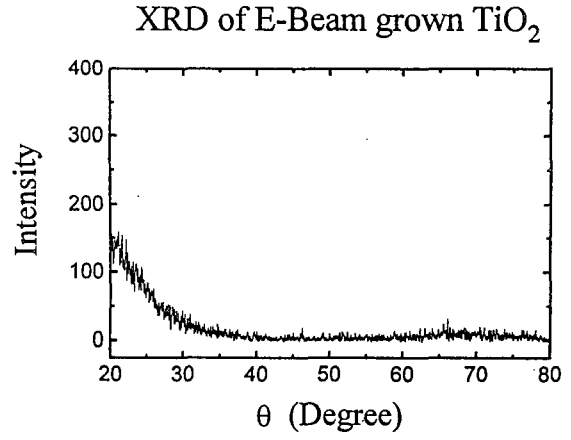

Fig. 5. The spectrum of a typical X-ray diffraction spectrum (θ-2θ) shows no sign of crystalline phase in the film.

quantum mechanical dispersion relation.[5] It is well known that a single oscillator could represent most amorphous materials, but the very broad plateau feature of the extinction coefficient between 4.5eV and 6.5eV strongly suggests multi-oscillator model will fit better than the previously employed single oscillator.[3] In the present work a double oscillator model is adopted and hence the following equation is used.

$$k(E) = \sum_{i=1}^{2} \frac{A_i(E-E_g)^2}{E^2-B_iE+C_i} \qquad (2)$$

where E is the photon energy and A_i, B_i, C_i ($i=1, 2$), E_g are the coefficients to be determined. With these coefficients and the refractive index at long wavelength n_∞, one can write the real part of the complex refractive index of TiO_2 film above the fundamental transition energy as given in Eq.(3).

$$k(E) = n_\infty + \sum_{i=1}^{2} \frac{B_iE-C_i}{E^2-B_iE+C_i} \qquad (3)$$

where

$$B_i = \frac{A_i(-B_i^2+2E_gB_i-2E_g^2+2C_i}{\sqrt{4C_i-B_i^2}} \qquad (4)$$

$$C_i = \frac{A_i[(E_g^2+C_i)B_i-4E_gC_i]}{\sqrt{4C_i-B_i^2}} \qquad (5)$$

n_∞ is determined so that the calculated refractive index in Eq.(3) matches the refractive index of the film at long wavelength limit. For a conventional electron beam grown TiO_2, the film refractive index at long wavelength is 2.191. The coefficients in Eq. (2) and n_∞ are copied into Table I.

The density of a film depends on film growth technique. The refractive index of a void containing film is low. The refractive index of a dielectric film is approximately proportional to the packing density of a film. The packing density of TiO_2 in film phase is less than that of the crystalline phase TiO_2. The refractive index of the conventional electron beam grown TiO_2 film at long wavelength, for an example, is about the same as that of anatase with 16% void in it. Considering that a dense TiO_2 film can be prepared with an improved film growth technique, the refractive index of a dense TiO_2 film has been calculated through an artificial inclusion of negative void into the current TiO_2 film. Thus the complex refractive index of a "void -free" TiO_2 in film phase, which possibly is the most dense amorphous TiO_2 in film phase, is used as the reference data of TiO_2 in film phase for a refined SE analysis.[4] The spectra of this complex refractive index are copied into Fig.6. The refractive indices averaged over three crystallographic directions, $(2n_o+n_e)/3$, of birefringent TiO_2 crystals (anatase and rutile) are plotted in the same graph for a comparison.

Table 1. The coefficients of the quantum mechanical dispersion relation and w n_∞ in Eq.(2) and Eq.(3).

A_1	B_1	C_1	A_2	B_2	C_2	F_g	n_∞
0.23	8.5	18.33	0.05	11.7	34.8	3.2	1.98

SE analysis is done as follow. Using the three phase model, the average thickness and the average void fraction can be determined. These are primary constants of the film. The surface microroughness information are substracted by replacing the three phase model with a four phase model, where a surface layer is introduced. Thus TiO_2 film is

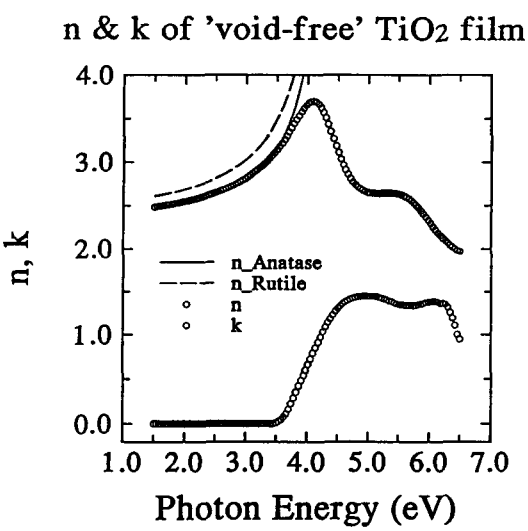

Fig. 6. The spectrum of the complex refractive index of the "void-free" TiO_2 in film phase. The refractive indices averaged over three crystallographic directions, $(2n_o+n_e)/3$, of birefringent TiO_2 crystals (anatase and rutile) are compared.

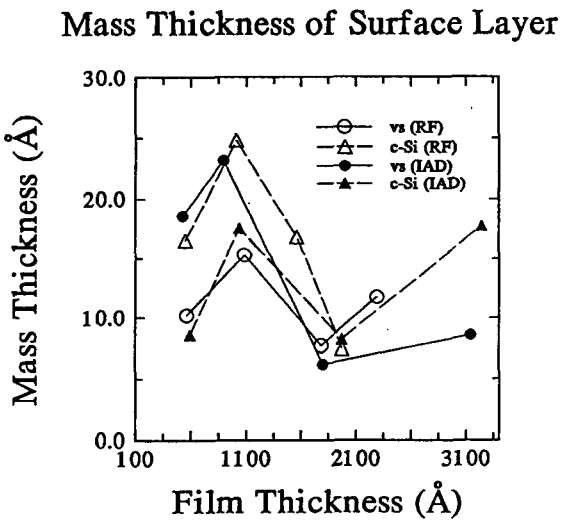

Fig. 7. The mass thickness of the micro-rough surface layer of TiO_2 films versus film thickness. It is lowest when the film thickness is about 2000 Å

simulated by the bulk film and a surface layer. Introduction of the four phase model improves fitting and reduces σ, the difference between the experimental and the calculated ellipsometric constants, but the values of the surface layer parameters are not satisfactory. The error bounds of both the thickness and the void fraction are abnormally large except for the conventional electron beam grown samples. This abnormally large error prohibits the extensive analysis of SE data, nevertheless a few valuable information on the surface microroughness has been substracted. The mass thickness of the surface layer defined as the volume fraction of TiO_2 multiplied by the thickness of the surface layer ranges from a few to a few tens of angstroms and is minimum when the thickness of TiO_2 film reaches 2000 Å. (Fig. 7) From AFM images, the SE analyzed surface microroughness of the conventional electron beam grown TiO_2 film is confirmed.

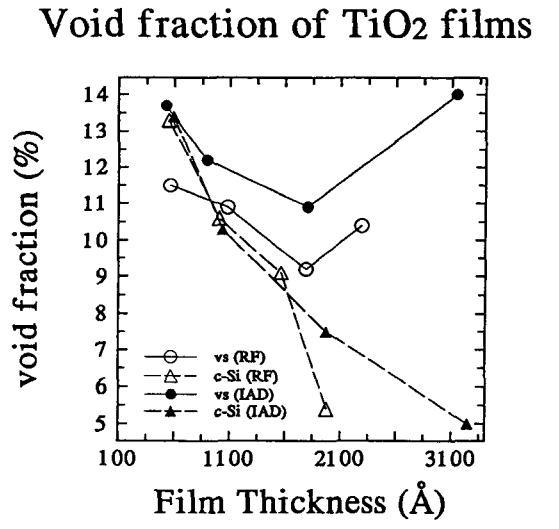

Fig. 8. The void fraction of TiO_2 films prepared by IAD and RF sputtering versus film thickness. These films have lower void fraction than those prepared by conventional electron beam deposition(19-24%, not shown in the graph). The void fraction of TiO_2 films on c-Si substrate (triangles) monotonically increases as the film thickness decreases, but for the film on vitreous silica substrate(circles), it shows a V shape with a minimum near 2000 Å

For the bulk films, the following observations worth mentioning. Average packing densities of TiO_2 films range from 76% to 95 %. Among them, IAD grown films and RF sputter grown films have lower void fraction of 5-14% (higher packing density of 86-95 %) than the conventional electron beam grown ones (19-24%). The observed void fraction of the films versus film thickness is shown in Fig. 8. It is interesting that the packing density of the films prepared on c-Si substrate by either technique of IAD or RF sputtering, monotonically increases from 87 % to 95% as the film grows from 500Å to 3200Å. On the other hand, the films prepared on vitreous silica substrate shows a V-shape void variation versus film thickness. The void fraction decreases from 12-14% at 500 Å and reaches its minimum value of 9-11% near 2000Å. After that it increases back to 14% at 3200Å. The three phase model parameters and the four phase model parameters determined by SE analysis are summarized into Table II.

The films of electron beam evaporation have higher void fraction and when it is placed on an humid enviroment for a prolonged period of time, the water vapor is

Table II. TiO_2 films prepared by a conventional electron beam deposition, IAD and RF sputtering deposition. The model parameters determined by SE analysis are also copied. The variation of void fraction of the films versus film thickness is shown in Fig. 7

No.	substrate	V_f(%)	D_f(Å)	σv_{bf}(Å)	d_{bf}(Å)	V_s(%)	d_s(Å)	σ	technipue	
R1-vs	SiO_2	11.5	562	0.079	10.8	551	46.4	19	0.069	RF
R2-vs	〃	10.9	1081	0.084	9.4	1053	41.2	26	0.068	〃
R3-vs	〃	9.2	1785	0.105	8.5	1767	40.7	13	0.104	〃
R4-vs	〃	10.4	2290	0.099	9.4	2259	41.3	20	0.091	〃
R1-Si	c-Si	13.3	552	0.061	12.6	528	36.5	26	0.043	〃
R2-Si	〃	10.6	1007	0.082	8.9	965	32.9	37	0.060	〃
R3-Si	〃	9.1	1561	0.108	7.4	1522	39.9	28	0.094	〃
R4-Si	〃	5.4	1974	0.139	5.1	1962	98.0	372	0.118	〃
I1-vs	SiO_2	13.7	526	0.063	12.9	504	33.7	28	0.050	IAD
I2-vs	〃	12.2	892	0.056	11.1	860	27.6	32	0.044	〃
I3-vs	〃	10.9	1802	0.086	10.5	1789	38.3	10	0.086	〃
I4-vs	〃	14.0	3145	0.092	13.3	3117	42.8	15	0.088	〃
I1-Si	c-Si	13.4	593	0.050	13.05	581	38.8	14	0.043	〃
I2-Si	〃	10.3	1036	0.076	0.9	1006	35.0	27	0.062	〃
I3-Si	〃	7.5	1973	0.110	6.7	1952	45.2	15	0.106	〃
I4-Si	〃	5.0	3246	0.255	0.5	3125	73.5	67	0.199	〃
E1-vs	SiO_2	23.8	1117	0.088	23.0	1100	70.7	64	0.051	EB
E1-Si	c-Si	18.9	1006	0.092	19.0	1006	97.7	46	0.092	EB[1]
		18.6	1065	0.130	14.4	983	45.2	63	0.043	EB[2]

1) measured on 9/15/94
2) measured on 10/1/95

known to condense into the micro-void. When this happens, the spectrum shifts to the longer wavelength region. The red shift of ellipsometric spectrum is observed. This condensed water is repelled from the microvoid by heating the specimen to 200℃ and keep it for a few hours in vacuum. The effect of water desorption on the ellipsometric constant is observed in real time by in-situ ellipsometry.(Fig. 9) At the very first run of this heating cycle, the water desorption from the micro-void of TiO_2 film continues, and hence the observed tan Ψ variation does not exactly follow the temperature variation (Fig. 9a), but after a few runs of heating cycle the water vapor is completely repelled out of the micro-void and tan Ψ variation follows quite silimar shape as the temperature variation.(Fig. 9b) Also it is confirmed that the ellipsometric spectrum blue-shifts back. After water desorption, the blue-shift of ellipsometric spectrum is observed.(Fig. 10)

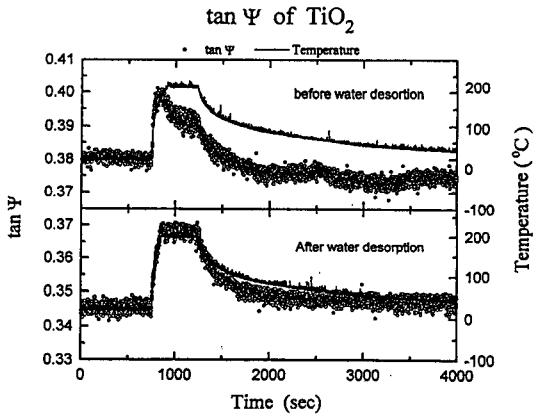

Fig. 9. The in-situ ellipsometric data(circles) (a) during water desorption and (b) after water desorption, out of the micro-void of the electron beam grown TiO_2 film when the heating cycle(solid line) is on.

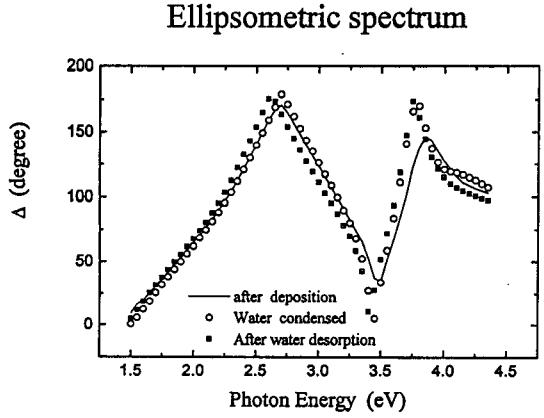

Fig. 10. The blue-shift of ellipsometric spectrum after the water desorption from the micro-void the electron beam grown TiO_2 film.

CONCLUSION

The complex refractive index of amorphous TiO_2 in film phase is obtained with the quantum mechanical dispersion constants as copied in Table I. Films prepared by RF magnetron sputtering and IAD shows the highest packing density (86-95%) whereas those by sol-gel method the lowest (76%). Surface microroughness ranges from a few angstroms to about 30 angstroms. The water condensation into the microvoid of TiO_2 film and water desorption out of it are observed in terms of red-shift and blue-shift of the ellipsometeric spectrum, respectively. The water desorption is also observed by in-situ, real time ellipsometry. AFM images confirmed SE modelling analysis and X-ray diffraction data.

ACKNOWLEDGEMENT

This paper was supported by Ajou University Special Research Support Program.

REFERENCE

1. H. A. Macleod, Thin-film optical filters, (Adam Hilger Ltd, Bristol, 1986) 391-393.
2. J. M. Bennett, E. Pelletier, G. Albrand, J. P. Borgogno, B. Lazarides, C. K. Carniglia, R.A. Schmell, T. H. Allen, T. Tuttle-Hart, K. H. Guenther, and A. Saxer, Applied Optics, **28**, 3303-3317 (1989).
3. S. Y. Kim, Applied Optics, (in press, 1996).
4. S. Y. Kim, H. J. Kim, H. M. Cho, and Y. W. Lee, SPIE, **2873**, 234-237 (1996).
5. A. R. Forouhi and I. Bloomer, Handbook of Optical constants of Solids II, Edward D. Palik, ed., (Academic Press, Inc., Toronto 1991) chap.7.
6. D. E. Aspnes, J. de Physique, **C10**, 3-12 (1983).